Design of a four-energy-level vertical external surface-emission laser enabled on the waveguide grating structure

Wenda Cui[a], **Hanchang Huang**[a], **Hongyan Wang**[b], **Kai Han**[a,b,*] **and Xiaojun Xu**[b,c]

[a]National University of Defense Technology, College of Advanced Interdisciplinary Studies, Changsha, China

[b]National University of Defense Technology, Interdisciplinary Center of Quantum Information, Changsha, China

[c]Hunan Provincial Key Laboratory of High Energy Laser Technology, Changsha, China

Abstract. Membrane or film gain mediums have attracted great attention for their good thermal performances and light field manipulation properties, which are helpful for the power scaling of a laser. A membrane laser enabled on the waveguide grating structure is proposed and this design is flexible to manipulate optical properties by controlling the photonic density of states. Lasing behavior is theoretically analyzed based on the four-level rate equations. Results show that pump absorption is enhanced by about 35 times, which leads to improved laser efficiency. When the laser mode overlaps the resonant guided mode, the Purcell factor achieves 212, leading to enhanced emission rate, as well as an apparent decrease of relaxation oscillating amplitude and time delay. The present work offers a preliminary design and lasing behavior analysis of the vertical external surface-emission laser enabled on the waveguide grating structure. [DOI: 10.1117/1.JNP.16.026003]

Keywords: subwavelength structures; gratings; gain membrane; lasers; absorption enhancement; emission enhancement.

Paper 21132G received Dec. 22, 2021; accepted for publication Apr. 12, 2022; published online May 4, 2022.

1 Introduction

It is the best time for the HPSSLs high-power solid-state lasers (HPSSLs) in recent decades, especially for the diode-pumped solid-state laser (DPSSL) because of its compact structure and good power-scalable ability. It is also a hard time for HPSSLs, although some laser systems have reached a high output power of several kilowatts,[1–3] they encounter a series of problems caused by the high power density in the gain medium, such as the thermal effects which could damage optical elements and worsen the beam quality. Fiber lasers, waveguide lasers, and thin disc lasers are now becoming the main candidates for HPSSLs. The fiber laser has a larger surface-to-volume ratio (SVR), whose cross-section radius is just several micrometers, so it has a quick waste heat dissipation and a simpler heat-removal system. Although high power fiber laser has better performances in some respects, its power increase has become slower in recent years because of the transverse mode instability and other nonlinear effects.[4] The planar waveguide laser (PWL) is another type of high-power solid-state laser, the width of which is usually several millimeters and its thickness is around tens or hundreds of micrometers. The output power of PWL has reached a multi-kilowatt level but the beam quality is not very well because it is not well restrained in one dimension.[5]

The cross-section radius of the thin disc laser is much larger than the fiber laser while its thickness is just hundreds of micrometers, so its SVR is almost as large as the fiber laser and it

*Address all correspondence to Kai Han, hankai0071@nudt.edu.cn

has a lower power density. On the other hand, thin disc lasers based on the vertical external surface-emitting architecture are capable of outputting a beam with a large mode area and high beam quality, which is very beneficial to HPSSL. The output power has been achieved 10-kW level,[6] however, when it comes down to higher power, its pump architecture and the manufacturing technology become very complicated, and the waste heat dissipation is much harder. The trend of thin-disk lasers is to further compress the thickness to pursue a higher heat dissipation rate. Recently, a membrane laser[7] of 0.59 μm thick has been developed; however, the round-trip pump absorption of the membrane is quite low because of its limited thickness.

The blossom of nanophotonics technology provides unique solutions to this problem. Lots of high efficiency and low threshold lasers have been realized based on special nanostructure design.[8–10] The photonic density of states (DOS) is affected by local light field distribution around the nanostructures, which is the key to these miniature light sources. Practically, by shape design of the gain medium or cavity, we can engineer or tailor the optical properties of these lasers. The guided-mode resonance (GMR), which permits field localization at the pump and lasing wavelength simultaneously, is a promising tool.[11–15] If the GMR is excited in the gain membrane, the absorption and emission properties could be improved artificially. Some simulation works of the membrane laser using GMR structure have been done, in which laser behavior is analyzed based on the rate equations.[16–18] Recently, a membrane laser based on the transmission GMR effect is proposed, in which two grating layers are used.[19] Some experimental works about the membrane laser are also conducted, in which the gain medium is the semiconductor membrane,[20] however, the GMR structure is not used so the vertical external surface-emitting cannot be realized.

The neodymium-doped material has been used as the gain medium widely in the high-power regime[21,22] and the Nd-doped film has been fabricated on different substrates by various methods.[23–26] The well-fabricated Nd-doped membrane has presented good optical properties and its intrinsic loss is quite low. Except for the thermal management advantage, the threshold of the Nd-doped membrane is lower meanwhile the optical efficiency is higher due to its four-energy-level system. Taking into account all the above advantages, we proposed a compound dielectric waveguide grating (CDWG) structure with the Nd-doped gain membrane as the waveguide layer. GMR is excited in the structure to enhance the pump absorption meanwhile lasing behavior is adjusted to obtain higher optical efficiency.

We first set up a model and gave optimized design parameters using the rigorous coupled-wave analysis (RCWA) method. In the waveguide layer, the light field was localized, so high absorption and emission enhancement were achieved. Second, we combined wave optical simulation with a four-level-rate-equation model and found laser efficiency improvement as well as a compress of relaxation oscillating. These results are particularly optimistic and will be useful for experimental laser scientists.

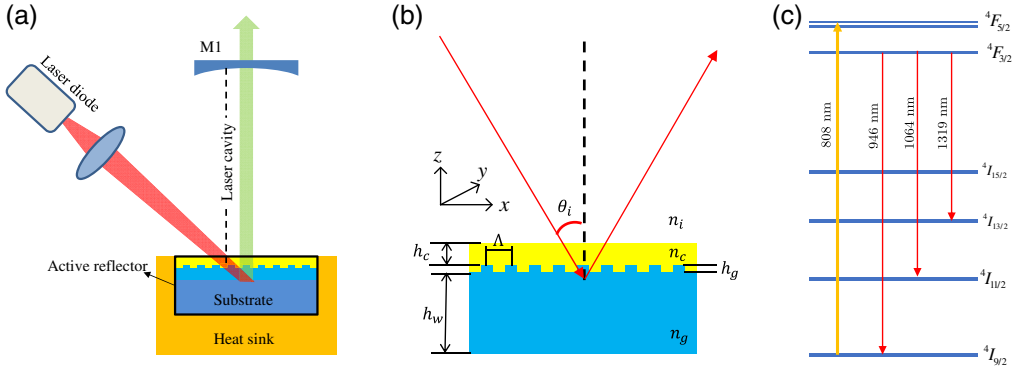

Fig. 1 The laser design with CDWG structure (a) the laser schematic, (b) the basic structure and parameters of the gain membrane, and (c) the four-energy level system of Nd^{3+} ions.

2 Laser Design with Gain Membrane Embedded in CDWG

The laser is designed as presented in Fig. 1(a). The whole CDWG structure is considered as an active reflector, which comprises a substrate and a nanostructure gain membrane. The substrate is used as the heat spreader and soldered on the heat sink with indium. As shown in Fig. 1(a), the parameters of the active reflector are optimized so that the laser mode could be overlapped by the GMR mode and the laser beam is highly reflected. M1 is used as the output coupling mirror and the reflection at laser wavelength is R. As a result, a vertical resonant cavity composed of M1 and the active reflector is built. Furthermore, the incident angle of the pump beam should also be optimized so that GMR mode could be excited at the pump wavelength.

Figure 1(b) shows the proposed nanostructure gain membrane. First, an Nd^{3+}-doped layer is deposited on the substrate, then a rectangular grating is etched on it. At last, a cap layer is fabricated on the top to protect the grating and improve the reflection spectrum. The Nd^{3+} doped film is considered the waveguide layer and its thickness is h_w. The depth of the grating section is h_g and the cap layer's thickness is h_c. Other physical factors are the grating period Λ and the filling factor f. The refractive indexes are $n_i = 1$, $n_c = n_s = 1.46$, and $n_g = 2.48$ (n_g is the gain film refractive index, n_i is the refractive index of incident area, and n_s is the substrate refractive index). As presented in Fig. 1(c), the pump transition rouses between the $^4I_{9/2}$ and $^4F_{5/2}$ levels while the emission transition is between the $^4F_{3/2}$ and $^4I_{11/2}$ levels. So M1 is coated with a reflection of 99.9% at 0.808 μm, and the laser beam at 1.064 μm is high reflected by the active reflector with the designed CDWG parameters.

The period structure in the CDWG is served as a Bragg reflector, so the incident plane wave can be diffracted into several orders. When an order with incident angle θ_i couples to the leaky mode supported by the waveguide layer, a GMR mode would be excited. Physically, 100% switching of optical energy between reflected and transmitted waves occurs with respect to the wavelength and angle of incidence.[27] These rapid variations of reflection or transmittance are also called GMR effects.

In the designed structure, when the diffracted pump or lasing beam [transverse magnetic (TM) polarization] overlaps the resonant mode, GMR is excited inside the waveguide layer, consequently, a narrow-width high reflection is obtained.[28] Light field is modified by the nanostructure, so lasing behavior would be different from a homogeneous gain medium. The light field $E(x, z)$ is calculated by the RCWA.[29] The RCWA method is a semi-analytical method that is frequently employed to solve the light field diffracted by a period structure. For the transverse electric (TE)-polarization light field, the incident normalized electric field is expressed as[30]

$$E_{\text{inc},y} = \exp[-jk_0 n_1(\sin\theta x + \cos\theta z)], \tag{1}$$

where $k_0 = 2\pi/\lambda_0$ and λ_0 is the wavelength of light in the region I. The normalized solutions in the region $I(z < 0)$ and region $II(z > d)$ are

$$E_{I,y} = E_{\text{inc},y} + \sum_i R_i \exp[-j(k_{xi}x - k_{I,zi}z)], \tag{2}$$

$$E_{II,y} = \sum_i T_i \exp\{-j[k_{xi}x - k_{II,zi}(z-d)]\}. \tag{3}$$

R_i is the normalized electric-field amplitude of the i'th reflected wave in region I. T_i is the normalized electric-field amplitude of the i'th transmitted wave in region II. d is the grating thickness, k_{xi} is determined from the Floquet condition, which is expressed as

$$k_{xi} = k_0[n_I \sin\theta - i(\lambda_0/\Lambda)]. \tag{4}$$

$k_{I,zi}$ and $k_{II,zi}$ are denoted as $k_{m,zi} = k_0\sqrt{n_m^2 - (k_{xi}/k_0)^2}(m = I, II)$. The electric and magnetic field in the grating region $(0 < z < d)$ is expressed as

$$E_{gy} = \sum_i S_{yi}(z)\exp(-jk_{xi}x), \tag{5}$$

$$H_{gx} = -j\left(\frac{\varepsilon_0}{\mu_0}\right)^{1/2}\sum_i U_{xi}(z)\exp(-jk_{xi}x). \tag{6}$$

Substituting Eqs. (5) and (6) and into Maxwell's equation and the normalized amplitude of the i'th space-harmonic fields $S_{yi}(z)$ and $U_{xi}(z)$ satisfy the coupled-wave equations, which are stated as

$$\frac{\partial S_{yi}}{\partial z} = k_0 U_{xi}, \tag{7}$$

$$\frac{\partial U_{xi}}{\partial z} = \left(\frac{k_{xi}^2}{k_0}\right)S_{yi} - k_0\sum_p \varepsilon_{(i-p)}S_{yp}. \tag{8}$$

The set of the coupled-wave equations can be solved by calculating the eigenvalues.[30,31] By matching the tangential electric and magnetic components at $z = 0$ and $z = d$ boundaries, the electromagnetic fields as well as R_i and T_i can be calculated. The diffraction efficiencies are defined as

$$\mathrm{DE}_{ri} = R_i R_i^* \mathrm{Re}\left(\frac{k_{I,zi}}{k_0 n_I \cos\theta}\right), \tag{9}$$

$$\mathrm{DE}_{ti} = T_i T_i^* \mathrm{Re}\left(\frac{k_{II,zi}}{k_0 n_I \cos\theta}\right). \tag{10}$$

For the TM polarization, the incident magnetic field is normal to the incidence plane, and the reflected and transmitted diffraction fields can also be calculated by solving similar eigenvalue equations. Diffraction efficiencies are defined as

$$\mathrm{DE}_{ri} = R_i R_i^* \mathrm{Re}\left(\frac{k_{I,zi}}{k_0 n_I \cos\theta}\right), \tag{11}$$

$$\mathrm{DE}_{ti} = T_i T_i^* \mathrm{Re}\left(\frac{k_{II,zi}}{n_{II}^2}\right) / \left(\frac{k_0 \cos\theta}{n_I}\right). \tag{12}$$

From the analysis, we can obtain the field distribution in the region I and region II by substituting R_i and T_i into Eqs. (2) and (3), the light field in the grating region can also be obtained by summing up the space harmonic items in Eqs. (5) and (6). Furthermore, by increasing the diffractive orders, high accuracy could be obtained.

On the other hand, a higher absorption could be obtained, which is beneficial for optical efficiency. The absorbance we obtained from the numerical simulation is defined as

$$A = 1 - (\sum_i R_i + \sum_i T_i). \tag{13}$$

The absorption could be calculated by introducing the complex refractive index data into the numerical model. A factor $M = A(\lambda)/[N_{\mathrm{ion}}\sigma_p(\lambda)h_w]$ is defined to indicate the enhanced absorption of the gain membrane with nanostructures, in which N_{ion} is the Nd^{3+} density and σ_p is its absorption cross-section.

Since the diffraction efficiency of a high order is lower, the grating period would better be smaller than λ_R/n. λ_R is the Rayleigh wavelength and n is the average refractive index of the waveguide layer. In Fig. 2(a), as the layer thickness increases, more GMR modes appear and high reflection arms get closer, which means that the resonant free-range gets shorter. As shown in Fig. 2(b), we optimized parameters of the CDWG structure as $h_w = 0.5$ μm, $h_g = 0.3$ μm, $h_c = 0.02$ μm, $f = 0.5$, and $\Lambda = 0.69$ μm. As each diffractive order couples to a leaky waveguide mode, there are many high reflection "arms" in the figure. Namely, there are many diffracted waves in the same direction exciting the GMR modes. On the other hand, some

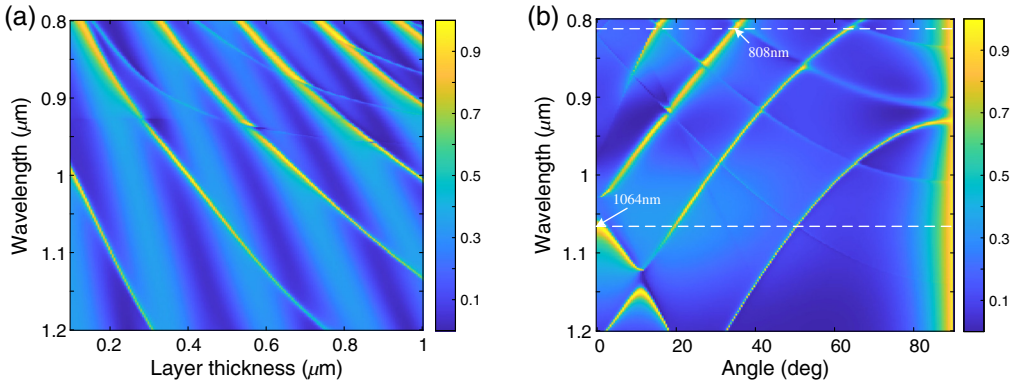

Fig. 2 Reflection maps with (a) different layer thicknesses and (b) different incident angles.

counterpropagating waves are also excited and enhanced simultaneously because of the perturbation of the grating. The counterpropagating waves interact with each other and result in spectrum splitting, which is also known as the resonance bandgap.[32] The dispersion curve is almost flat at the edge of band gaps, so the reflection would keep high at a fixed wavelength as the incident angle changes. That is to say, the angle tolerance is improved, which is beneficial to assemble the laser cavity. As the parameters of the compound structure change, the band gaps will shift so appropriate resonant wavelength for the pump and emission light can be obtained with carefully chosen parameters. In Fig. 2(b), it is apparent that some GMR modes appear when the wavelength $\lambda = 808$ nm and $\lambda = 1064$ nm. According to the laser schematic designed in Fig. 1(a), the laser beam in the cavity oscillates vertically to the active reflector, so the resonant angle is chosen as $\theta_i = 0$ deg. Similarly, the resonant angle of the pump beam with the wavelength $\lambda = 808$ nm is larger than 0 deg. Reflection curves in Fig. 3(a) are exacted from Fig. 2(b), and present a high reflection of 99.8% at 1.064 μm when the incident angle $\theta_i = 0$ deg, as well as a reflection of 98% at 0.808 μm when the incident angle $\theta_i = 35.7$ deg. It can be deduced from Fig. 1(a) that a higher reflection at the wavelength $\lambda = 1.064$ μm is beneficial for the laser design, which means the cavity loss would be lower.

As GMR is excited at the pump wavelength, Fig. 3(b) presents the absorption factor M, which achieves about 35 at 0.808 μm. The absorption enhancement is due to the light field localization in the waveguide layer as shown in Fig. 4(a), as a result, more Nd^{3+} ions could be pumped to the excited state.

Besides the absorption, the confined light field in the CDWG structure also affects the emission enhancement apparently known as the Purcell effect. The Purcell factor F is defined as[33]

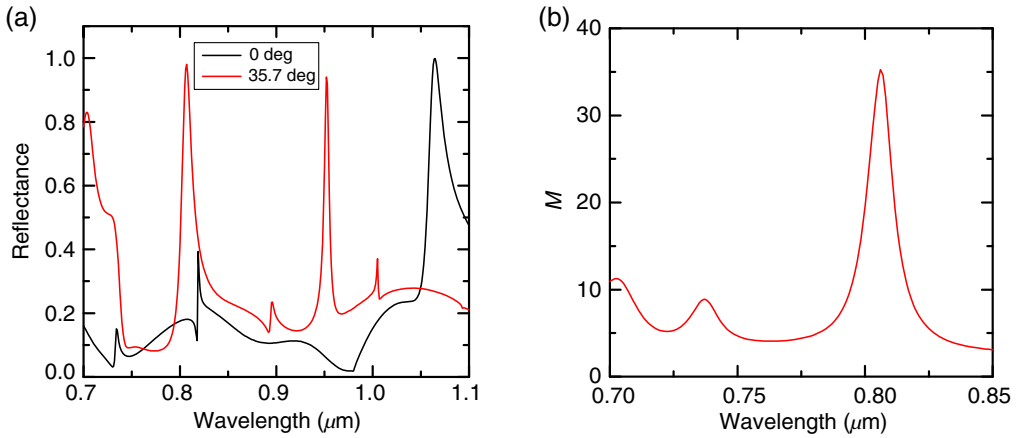

Fig. 3 (a) The reflectance spectrum of beams with different incident angles and (b) the absorption enhancement.

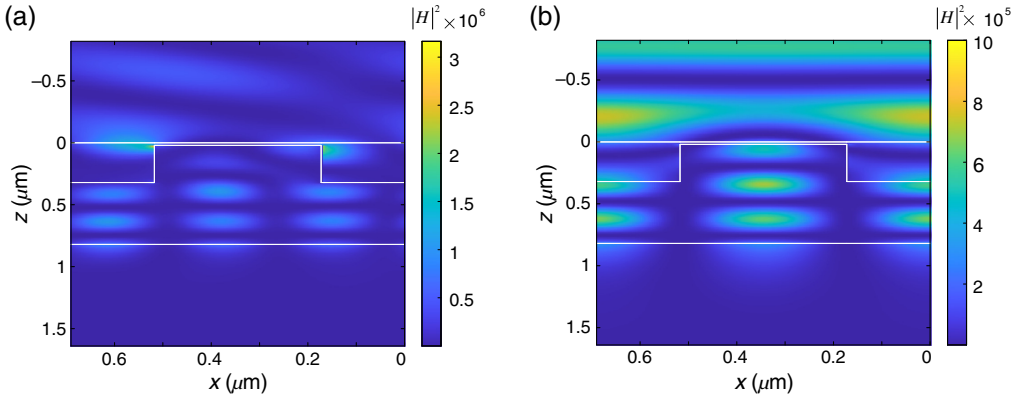

Fig. 4 Light field distribution with (a) $\lambda = 808$ nm, $\theta = 35.7$ deg and (b) $\lambda = 1064$ nm, $\theta = 0$ deg.

$$F = \frac{3}{4\pi^2}\left(\frac{Q}{V_m}\right)\left(\frac{\lambda}{n}\right)^3. \tag{14}$$

Q is the quality factor, which could be obtained by $Q = \lambda/\Delta\lambda$. λ is the laser wavelength, $\Delta\lambda$ is the line width, n is the refractive index, and V_m indicates the mode volume defined as

$$V_m = \frac{\int_V \varepsilon(r)|E(r)|^2 \mathrm{d}^3 r}{\max[\varepsilon(r)|E(r)|^2]} \tag{15}$$

(r) is the permittivity at position r and $E(r)$ is the light amplitude. In Fig. 3(a), the spectral width of the GMR mode at $\lambda = 1.064$ μm is suppressed apparently. Namely, the photonic density of final states ρ is enhanced. As the DOS $\rho = 1/(\Delta\nu V_m)$, in which $\Delta\nu$ is the line width of the GMR mode, the transition between $^4F_{3/2}$ and $^4I_{11/2}$ would be enhanced according to Fermi's gold rule.[34] As shown in Fig. 4(b), the light field of $\lambda = 1.064$ μm is enhanced apparently in the waveguide layer. By introducing refractive index and light amplitude distribution into Eqs. (14) and (15), $F = 212$ is obtained. Lasing behavior affected by the GMR effect is analyzed in detail in the next section.

3 Lasing Behavior of the Designed Membrane Laser

The Nd^{3+}-doped gain medium is a four-energy-level system as Fig. 1(c) shows. Since the relaxation process between $^4F_{5/2}$ and $^4F_{3/2}$ is extremely fast, means that the light field localization mainly affects the stimulated absorption process instead of the spontaneous emission between $^4F_{5/2}$ and $^4I_{9/2}$. On the other hand, the lifetime of $^4F_{3/2}$ is about 200 μs, so the emission process is apparently affected by the Purcell effect. As the light and gain material interaction is enhanced by the structure design in the last section, we analyzed the lasing dynamic progress based on the rate equations, which are given as

$$\frac{dn_4}{dt} = R_p - \frac{n_4}{\tau_{43}}, \tag{16}$$

$$\frac{dn_3}{dt} = \frac{n_4}{\tau_{43}} - \frac{n_3}{\tau'_{32}} - R_{\mathrm{se}}, \tag{17}$$

$$\frac{dn_2}{dt} = \frac{n_3}{\tau'_{32}} - \frac{n_2}{\tau_{21}} + R_{\mathrm{se}}, \tag{18}$$

$$\frac{dn_1}{dt} = \frac{n_2}{\tau_{21}} - R_p. \tag{19}$$

n_i ($i = 1,2,3,4$) is the ion density of different energy levels, $R_p = I_p \eta_{\text{abs}}/h_w$ is the pump rate and η_{abs} is the absorption coefficient. In this model, the gain thickness h_w is so small that the absorption coefficient could be defined as $\eta_{\text{abs}} = 1 - \exp(-M\sigma_a n_0 h_w)$. n_0 is the doped Nd^{3+} ion density, M is the absorption enhancement factor, and σ_a is the absorption cross-section. τ_{43} and τ_{21} indicate the lifetime of non-radiative transitions. In the four-energy-level system of Nd^{3+} ions, the relaxation process τ_{43} and τ_{21} are not affected while the lasing process is enhanced by the Purcell effect between the $^4F_{3/2}$ to $^4I_{11/2}$ transition. The effective lifetime of $^4F_{3/2}$ is defined as $\tau'_{32} = \tau_{32}/F$, which means the spontaneous rate is much higher.

The stimulated emission rate R_{se} can be expressed by Eq. (20) for the homogeneous broadening, which is given as

$$R_{\text{se}} = \Delta n \frac{v^3 F}{4\pi^2 \tau_{32} \nu_0^2 \Delta\nu} \phi, \tag{20}$$

$\Delta\nu$ is the full-width at half-maximum of the Lorentzian spectral line shape function, ν is the group velocity in the dielectric medium and ν_0 is the central frequency. $\Delta n = (n_3 - f' n_2)$ is the population reversion, and f' is the Boltzmann population factor between the $^4F_{3/2}$ and $^4I_{11/2}$ level, which is about 6.17×10^{-7} at room temperature. We assume that only the resonance modes overlapping with the modes of the spontaneous emission relax with a shorter lifetime τ'_{32}. ϕ is the photon density in the cavity and satisfies the Eq. (21), which is

$$\frac{d\phi}{dt} = R_{\text{se}} - \frac{\phi}{\tau_r} + a\frac{n_3}{\tau'_{32}}. \tag{21}$$

The photon density is mainly affected by three factors: the stimulated emission, the photon loss, and the spontaneous emission in the cavity. τ_r is the photon lifetime that represents the photon loss and can be expressed as $\tau_r = 2L'/[c(\delta - \ln(R))]$, δ is the round-trip loss including the medium loss, the diffraction loss, and the mirror absorption. Especially in this model, δ mainly depends on the reflection of the CDWG structure at 1064 nm. L' is the effective optical length $L' = n_g l + n_g(l - l)$, l is the gain thickness and L is the cavity length. a denotes the ratio of the contribution that the spontaneous emission makes to the laser oscillation.

Since pump absorption is enhanced because of the field localization in the waveguide layer, the stimulated absorption is improved by about 35 times with the pump beam incident at an appropriate angle of 35.7 deg as presented in Fig. 3(b). Parameters used in the paper are listed in Table 1.[35,36]

The slope efficiency and the temporal characteristics are shown in Fig. 5. The Purcell factor F and the enhancement factor M are calculated in the last section. The Nd^{3+} density is $n_0 = 1.38 \times 10^{20}$ cm^{-3}.

Figure 5(a) shows the relationship between the output power intensity and the pump intensity with different F and M values. For the designed membrane laser with the Purcell factor $F = 212$ and absorption enhancement factor $M = 35$, the pump threshold is lower, and the optical

Table 1 Parameters used in the four-energy-level calculation.

Relaxation time ($^4F_{5/2} - {}^4F_{3/2}$) τ_{43}	0.2 ns
Relaxation time ($^4I_{11/2} - {}^4I_{9/2}$) τ_{21}	0.5 ns
Absorption cross-section (808 nm) σ_a	1.39×10^{-20} cm^2
Emission cross-section (1064 nm)	3.55×10^{-19} cm^2
Reflection of coupling mirror	0.43
Round-trip loss	0.1
Contribution ratio of the spontaneous emission a	0.1

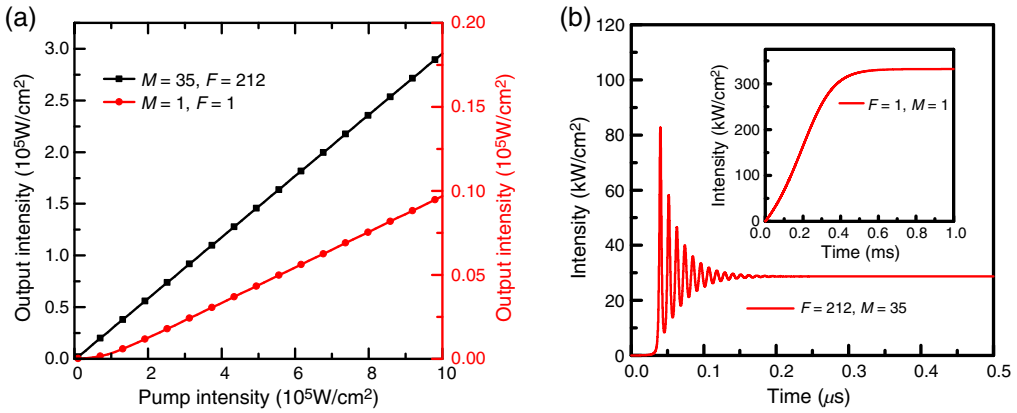

Fig. 5 Output power characteristics: (a) output power with $M = 1$, $F = 1$, and $M = 35$, $F = 212$ and (b) temporal output power with $M = 1$, $F = 1$ and $M = 35$, $F = 212$.

efficiency is much higher than a classic laser based on a homogenous gain medium without nanostructure ($M = 1$ and $F = 1$). As shown in Fig. 4(a), light field enhancement in the gain medium is realized by design, so the stimulated absorption, which is proportional to the light intensity, is greatly enhanced. As a result, more Nd^{3+} ions are excited to the $^4F_{3/2}$ energy level in the gain medium and the inverted population density Δn gets higher. Considering Eqs. (20) and (21), more stimulated emission photons can be obtained while the excited ions transmit to the ground state $^4I_{11/2}$. Consequently, a high enough gain coefficient could be enabled by less pump power to achieve laser oscillation and emit higher laser power.

On the other hand, with the pump intensity $I_p = 1 \times 10^5$ W/cm^2, the output lasing process is shown in Fig. 5(b) and the inset figure presents the lasing process with $M = 1$ and $F = 1$. The laser relaxation achieved a steady state at about 580 μs without nanostructure ($M = 1$ and $F = 1$) and about 0.29 μs with the designed nanostructure ($M = 35$ and $F = 212$). A larger M means that a higher pump rate is obtained, which corresponds to a shorter time to achieve a steady-state. Namely, while the laser mode overlaps the resonant mode in the CDWG, the lasing oscillation starts much more quickly than $F = 1$. Further analysis of the impact of the M and F factor is presented in Fig. 6.

The black line in Fig. 6(a) shows the changing of the maximum lasing relaxation intensity in the cavity while the absorption enhancement factor M increases from 1 to 50. The F factor is set as a constant of 212 in Fig. 6(a). A higher M means that more pump power is absorbed and R_p gets larger. According to the rate Eqs. (16)–(19), more ions can be pumped to the $^4F_{3/2}$ energy level, as a result, the inverted population density Δn gets higher. Considering Eqs. (20) and (21), the stimulated rate R_{se} gets higher and the photon density in the cavity will increase consequently.

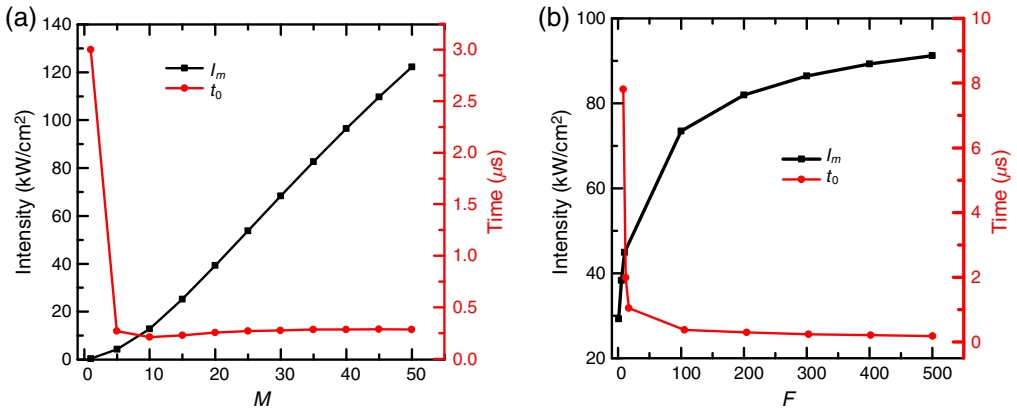

Fig. 6 Lasing relaxation amplitude and lifetime with increasing (a) M and (b) F values.

On the other hand, the relaxation lifetime t_0, which is defined as the time that the laser relaxation cost to achieve a steady outputting, is dramatically decreased as the red line presents in Fig. 6(a). The relaxation lifetime is about 3μs for $M = 1$, when the M factor equals 5, the lifetime is shortened to about 0.27 μs and changes little with the further increase of the M factor. According to the rate Eqs. (16)–(19), a small M factor means that fewer ions are pumped to the excited state, so the stimulated rate R_{se} is subsequently much lower. Referring to Eq. (21), a lower R_{se} means that the spontaneous emission provides more photons than the stimulated emission in the cavity. Since the power increase of stimulated emission is much faster than that of the spontaneous emission, the laser intensity in the cavity will increase slowly and the relaxation lifetime is longer.

The black line in Fig. 6(b) shows the changing of the maximum lasing relaxation intensity in the cavity while the Purcell factor F increases from 1 to 500. The M factor is set as a constant of 35 in Fig. 6(b). According to Eq. (20), the stimulated emission rate R_{se} will get higher while the Purcell factor increases. As a result, the photon density in the cavity will increase just like the situation in Fig. 6(a). On the other hand, since the effective lifetime of $^4F_{3/2}$ is defined as $\tau'_{32} = \tau_{32}/F$, the spontaneous rate will be much higher with a larger F factor. According to Eq. (21), the stimulated emission and spontaneous emission process get faster simultaneously in the cavity, so the relaxation lifetime decreases dramatically as the red line presents in Fig. 6(b).

4 Conclusions

A membrane laser is designed based on the CDWG structure, in which the Nd-doped film is used as the gain medium as well as part of the CDWG structure that rouses the light field localization. Proper parameters of the CDWG structure are optimized carefully to achieve high reflection at both the pump and laser wavelength. The pump beam is efficiently absorbed, and the stimulated emission process is accelerated either, which may make sense to realize a high-efficiency and quick response laser. These results mean that nanotechnology could play a great role in solid-state lasers, which will be particularly helpful for high energy laser scientists, and this needs more participation of nano-scientists.

Acknowledgments

We thank Zining Yang (National University of Defense Technology, College of Advanced Interdisciplinary Studies) for the helpful discussions and Maohui Yuan (National University of Defense Technology, Interdisciplinary Center of Quantum Information) for the English editing. The authors declare that they have no known competing financial interests or personal relationships that could have appeared to influence the work reported in this paper.

Code, Data, and Materials Availability

The data and codes used or analyzed during the current study are available from the corresponding author on reasonable request.

References

1. T. Gottwald et al., "Recent disk laser development at Trumpf," *Proc. SPIE* **8547**, 85470C (2012).
2. B. Yang et al., "4.05 kW monolithic fiber laser oscillator based on home-made large mode area fiber Bragg gratings," *Chin. Opt. Lett.* **16**, 031407 (2018).
3. IPG photonics, "The world's smallest kW-class fiber lasers," The World's Smallest kW-class Fiber Lasers, https://www.ipgphotonics.com/en/products/lasers/mid-power-cw-fiber-lasers/1-micron/ylr-u-series (2022).
4. J. Richardson, J. Nilsson, and W. A. Clarkson, "High power fiber lasers: current status and future perspectives [Invited]," *J. Opt. Soc. Am. B* **27**, B63–B92 (2010).

5. D. Filgas et al., "Recent results for the Raytheon RELI program," *Proc. SPIE* **8381**, 83810W (2012).
6. A. Giesen and J. Speiser, "High-power thin disk lasers," *Proc. SPIE* **8547**, 85470B (2012).
7. H. Kahle et al., "Semiconductor membrane external-cavity surface-emitting laser (MECSEL)," *Optica* **3**(12), 1506–1512 (2016).
8. M. Srinivas Reddy et al., "Low-threshold lasing in photonic-crystal heterostructures," *Opt. Express* **22**, 6229–6238 (2014).
9. S. Bao et al, "Low-threshold optically pumped lasing in highly strained germanium nanowires," *Nat Commun.* **8**, 1845 (2017).
10. M. Khajavikhan et al., "Thresholdless nanoscale coaxial lasers," *Nature* **482**, 204–207 (2012).
11. W. Cui et al., "High efficiency quasi-three level thin film laser enabled on a sinusoidal grating substrate," *Opt. Express* **25**(4), 4097–4105 (2017).
12. A. S. D. Sandanayaka et al., "Toward continuous-wave operation of organic semiconductor lasers," *Sci. Adv.* **3**(4), e1602570 (2017).
13. J. H. Lin et al., "Giant enhancement of upconversion fluorescence of $NaYF_4$:Yb^{3+}, Tm^{3+} nanocrystals with resonant waveguide grating substrate," *ACS Photonics* **2**(4), 530–536 (2015).
14. J. H. Lin et al., "Guided-mode resonance enhanced excitation and extraction of two-photon photoluminescence in a resonant waveguide grating," *Opt. Express* **21**(20), 24318–24325 (2013).
15. Y. Liu et al., "Broadband antireflection and absorption enhancement by forming nanopatterned Si structures for solar cells," *Opt. Express* **19**(s5), A1051–A1056 (2011).
16. K. Wang et al., "Enhanced lasing behavior enabled by guided-mode resonance structure embedded with double waveguide layers," *Appl. Opt.* **59**, 6113–6118 (2020).
17. Z. Zhang et al., "Controllable lasing behavior enabled by compound dielectric waveguide grating structures," *Opt. Express* **24**, 19458–19466 (2016).
18. X. Zhang et al., "Low-threshold nanolaser based on hybrid plasmonic waveguide mode supported by metallic grating waveguide structure," *Nanomaterials* **11**, 2555 (2021).
19. K. Wang et al., "Controllable lasing behavior enabled by the transmission guided-mode resonance effect in coupled gratings," *Opt. Commun.* **511**, 128010 (2022).
20. B. Jeżewski et al., "Membrane external-cavity surface-emitting laser emitting at 1640 nm," *Opt. Lett.* **45**, 539–542 (2020).
21. H. Norman, J. G. Douglas, and B. E. Dietmar, "Efficient high-power operation at 1.44 μm of Nd-doped crystals," *Proc. SPIE* **2206**, 426–436 (1994).
22. J. Lu et al., "Optical properties and highly efficient laser oscillation of Nd:YAG ceramics," *Appl. Phys. B* **71**, 469–473 (2000).
23. M. Nistor, F. Gherendi, and J. Perrière, "Tailorable properties of Nd-doped ZnO epitaxial thin films for optoelectronic and plasmonic devices," *Opt. Mater.* **126**, 112154 (2022).
24. M. Nistor et al., "Nd-doped ZnO films grown on c-cut sapphire by pulsed-electron beam deposition under oblique incidence," *Appl. Surf. Sci.* **563**, 150287 (2021).
25. S. Barsanti et al., "Nd3+-doped fluoride film grown on LiYF4 substrate by pulsed laser deposition," *Thin Solid Films* **516**, 2009–2013 (2008).
26. P. A. Atanasov et al., "Luminescence properties of thin films prepared by laser ablation of Nd-doped potassium gadolinium tungstate," *Appl. Phys. A* **74**, 109–113 (2002).
27. S. S. Wang et al., "Guided-mode resonances in planar dielectric-layer diffraction gratings," *J. Opt. Soc. Am. A* **7**, 1470–1474 (1990).
28. Z. S. Liu and R. Magnusson, "Concept of multiorder multimode resonant optical filters," *IEEE Photonics Technol. Lett.* **14**(8), 1091–1093 (2002).
29. L. Li and C. W. Haggans, "Convergence of the coupled-wave method for metallic lamellar diffraction gratings," *J. Opt. Soc. Am. A* **10**(6), 1184–1189 (1993).
30. M. G. Moharam et al., "Formulation for stable and efficient implementation of the rigorous coupled-wave analysis of binary gratings," *J. Opt. Soc. Am. A* **12**, 1068–1076 (1995).
31. S. Peng and G. M. Morris, "Efficient implementation of rigorous coupled-wave analysis for surface-relief gratings," *J. Opt. Soc. Am. A* **12**, 1087–1096 (1995).

32. T. Sun et al., "Dispersion relation of guided-mode resonances in multimode grating waveguide structures," *J. Mod. Opt.* **57**(10), 901–907 (2010).
33. E. M. Purcell, "Spontaneous emission probabilities at radio frequencies," *Phys. Rev.* **69**(11), 681 (1946).
34. E. Fermi, *Nuclear Physics*, University of Chicago Press (1950).
35. M. F. Joubert et al., "A spectroscopic study of $NaYF_4:Nd^{3+}$," *J. Lumin.* **51**(4), 175–187 (1992).
36. L. D. Deloach et al., "Evaluation of absorption and emission properties of Yb^{3+} doped crystals for laser applications," *IEEE J. Quantum Electron.* **29**(4), 1179–1191 (1993).

Biographies of the authors are not available.